Drops on the Underside of a Slightly Inclined Wet Substrate Move Too Fast to Grow

Etienne Jambon-Puillet,[1] Pier Giuseppe Ledda,[2] François Gallaire,[2] and P.-T. Brun[1]
[1]Department of Chemical and Biological Engineering, Princeton University, Princeton, New Jersey 08540, USA
[2]Laboratory of Fluid Mechanics and Instabilities, Ecole Polytechnique Fédérale de Lausanne, Lausanne CH-1015, Switzerland

(Received 10 December 2020; revised 15 April 2021; accepted 16 June 2021; published 23 July 2021)

Pendant drops suspended on the underside of a wet substrate are known to accumulate fluid from the surrounding thin liquid film, a process that often results in dripping. The growth of such drops is hastened by their ability to translate over an otherwise uniform horizontal film. Here we show that this scenario is surprisingly reversed when the substrate is slightly tilted (≈2°); drops become too fast to grow and shrink over the course of their motion. Combining experiments and numerical simulations, we rationalize the transition between the conventional growth regime and the previously unknown decay regime we report. Using an analytical treatment of the Landau-Levich meniscus that connects the drop to the film, we quantitatively predict the drop dynamics in the two flow regimes and the value of the critical inclination angle where the transition between them occurs.

DOI: 10.1103/PhysRevLett.127.044503

Anyone who has applied paint to a ceiling knows that thin liquid coatings can spontaneously destabilize and accumulate into an array of pendant drops [1,2]. While interfacial instabilities can be harnessed to build structures akin to geomorphic patterns [3–8], the Rayleigh-Taylor instability in films is more commonly seen as undesirable, e.g., jeopardizing the uniformity of coatings [9]. Worse, as they grow, instability-mediated drops can drip and pollute the space underneath, with potentially severe consequences for engineering constructs [10,11]. As such, the Rayleigh-Taylor instability in thin viscous films has been extensively studied [1,2,12–14] and diverse strategies have been proposed to prevent the formation of drops [15–21]. Linear stability analysis for this class of problems is therefore well established, while insights in the drop patterns formed by the instability have been provided using weakly nonlinear developments [2]. Yet, our understanding of fully formed pendant drops and their transition to dripping remains sparse [22] owing to the difficulties of modeling the fully nonlinear long-term dynamics. In this Letter, we focus on a single pendant drop (see Fig. 1), a problem that remains analytically tractable while retaining a rich physics.

Pendant drops under uniformly coated films are capable of steady translation, even in the theoretical limit of a perfectly horizontal substrate [22]. Over the course of their trajectory, these drops accumulate more fluid from the surrounding thin film than if they were stationary [22], thereby reaching the critical size leading to dripping [4] faster than immobile drops. Here, using experiments, numerical simulations, and theory, we show that increasing the drop velocity by slightly tilting the substrate surprisingly prevents dripping. Past a critical inclination, the film left by the drop in its wake is thicker than the one absorbed by the drop in its front. This negative balance depletes the volume of fluid in the drop, which shrinks, thereby avoiding dripping. Through an analysis of the Landau-Levich meniscus at the edge of the drop, we unveil the physics at play in these drops that are too fast to grow and predict analytically their dynamics and the transition between the two aforementioned flow regimes.

Our experiment is schematized in Fig. 1. Silicone oil (density $\rho = 971$ kg/m^3, surface tension $\gamma = 20.3$ mN/m, viscosity $\eta = 1.13$ Pa s) is spin coated on a flat glass substrate to produce a film of uniform thickness h_0 (measured by weighing the sample). The substrate is then flipped and mounted onto a rotating arm while a droplet is applied on the film with a micropipette. The resulting pendant drop has an initial amplitude $A_0 \sim \ell_c$, where $\ell_c = \sqrt{\gamma/(\rho g)}$ denotes the capillary length and g denotes the acceleration of gravity. The substrate is then tilted by an angle α and the dynamics is recorded (see Supplemental Material, Sec. I for details [23]). Note that the initial coating is sufficiently thin not to destabilize via the Rayleigh-Taylor instability over the course of our experiment [2]. The film thickness is therefore assumed to be uniform and constant far from the drop.

Figure 2(a) shows a chronophotography of an experiment performed with a nearly horizontal substrate

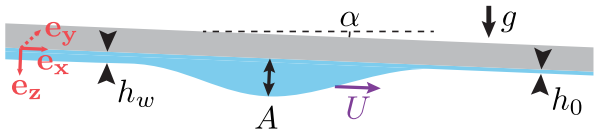

FIG. 1. Schematic of a pendant drop of amplitude A sliding with velocity U under a substrate prewetted with a film of thickness h_0 and inclined by an angle α.

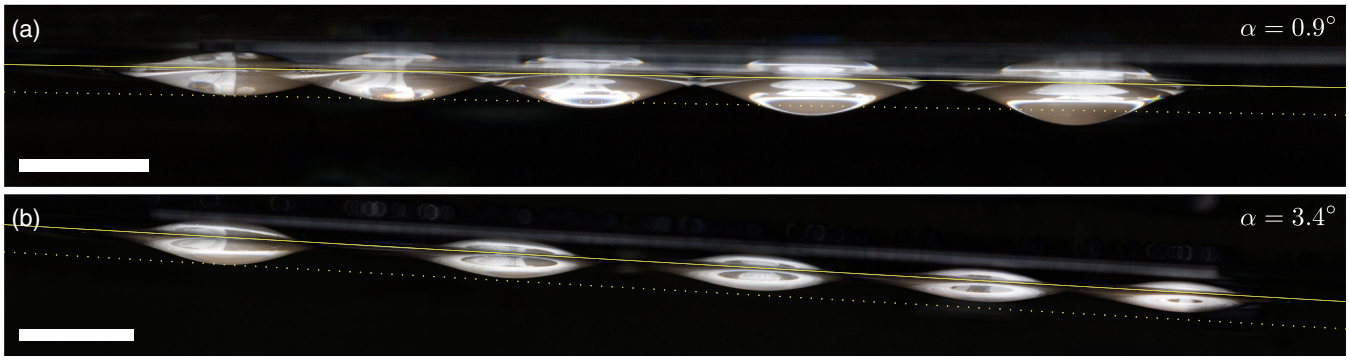

FIG. 2. Chronophotographies of two experiments at low (a) and high (b) inclination angles with $h_0 \approx 89$ μm (scale bars are 5 mm). The interval between pictures is 9 and 3.75 min, respectively. The pictures include the reflection of the drop on the substrate. The solid lines indicate the position of the substrate. The dotted lines mark the initial amplitudes of the drops $A_0 = \{1.03, 1.16\}$ mm.

($\alpha = 0.9°$). As evident from the figure, the drop translates by several times its diameter over the course of the experiment, while both the drop speed U and amplitude A increase. In Fig. 2(b), we show an experiment nearly identical to Fig. 2(a), except for that the inclination angle is slightly higher ($\alpha = 3.4°$). As expected, the drop initially moves faster. However, unlike the lower inclination case, it progressively shrinks and decelerates. In Fig. 3, we plot the amplitude $A(t)$ and position $x(t)$ of drops sliding over films of similar thickness ($h_0 \approx 89$ μm) but with different inclination angles α. Whereas the drop accelerates and grows for the three smallest angles, the situation is reversed for the two largest angles. The inclination $\alpha_c \approx 2°$ appears to be the critical angle α_c, where the drop amplitude and speed are constant ($U \approx 2.3$ mm/ min). Video S1 in the Supplemental Material [23] displays similar observations for $h_0 \approx 112$ μm. Modifying the film thickness changes the value of α_c, as well as the timescale of the experiment. Increasing the drop initial amplitude A_0 appears to speed up the dynamics, but does not change its outcome (see Supplemental Material, Sec. II [23]).

We turn to numerical simulations to rationalize these two flow regimes. Owing to the dimensions of the problem, we use the lubrication approximation to describe the evolution of the position of the interface $h(x, y, t)$ [1], but retain the full-fledged expression of the curvature κ [14,24]. In the Cartesian frame aligned with the substrate (see Fig. 1), we obtain the following dimensionless thin-film equation after rescaling x and y using $\ell_c/\sqrt{\cos\alpha}$, h using the coating thickness far from the drop h_0, and t using $\tau = \eta\gamma/(h_0^3\rho^2 g^2 \cos^2\alpha)$:

$$\partial_{\bar{t}}\bar{h} + \tilde{\alpha}\bar{h}^2\partial_{\bar{x}}\bar{h} + (1/3)\bar{\boldsymbol{\nabla}}\cdot[\bar{h}^3(\bar{\boldsymbol{\nabla}}\bar{h} + \bar{\boldsymbol{\nabla}}\bar{\kappa})] = 0,$$
$$\bar{\kappa} = \bar{\boldsymbol{\nabla}}\cdot\left[\bar{\boldsymbol{\nabla}}\bar{h}/\sqrt{1 + (h_0\sqrt{\cos\alpha}/\ell_c)^2(\bar{\boldsymbol{\nabla}}\bar{h})^2}\right], \qquad (1)$$

where a bar indicates rescaled variable. Note that the inclination of the substrate is captured by $\tilde{\alpha} = \ell_c \tan\alpha/h_0\sqrt{\cos\alpha} \approx \ell_c\alpha/h_0$.

We solve Eq. (1) with the finite element software COMSOL on a rectangular domain with periodic boundary conditions and the initial condition $\bar{h}(\bar{x}, \bar{y}, 0) = 1 + h_d(\bar{x}, \bar{y})/h_0$. Here, $h_d(\bar{x}, \bar{y})/\ell_c$ is the dimensionless profile of a static pendant drop obtained by integrating the Young-Laplace equation numerically (see Supplemental Material, Sec. I for numerical details [23]). In Video S2, we report typical numerical results, which appear qualitatively similar to experiments, i.e., predicting growth and ultimately dripping at low inclination angles and the opposite at higher angles. In Fig. 3, we show the evolution of the drop amplitude $A(t)$ and position $x(t)$ obtained numerically with the parameters corresponding to the aforementioned experiments within their uncertainty ($\Delta h_0 = 7$ μm, $\Delta\alpha = 0.15°$). The agreement between experiments and numerics is favorable, thereby validating our simulations.

Leveraging our simulations, we investigate the physics setting the value of the critical angle α_c. In Fig. 4(a), we plot side by side the log of the dimensionless film thickness $h(x, y)/h_0$ for two drops, each of which corresponds to a given flow regime. The two situations only differ in the value of the dimensionless inclination angle $\tilde{\alpha}$. Yet, their respective wakes are qualitatively different. In particular, the wake thickness h_w appears to be mostly greater than h_0 for large inclinations and lower than h_0 for small inclinations. This sizable difference plays a key role in defining the flow regimes. Along its trajectory, a drop indeed absorbs the uniform film laying at its front and releases liquid in its wake. The contribution from the Rayleigh-Taylor instability being negligible (see Fig. S3 in the Supplemental Material [23]), the change in volume of the drop is $\partial_x V \approx \int_{-R}^{R}[h_0 - h_w(y)]dy$ with R as the drop radius. The drop shrinks if $\partial_x V < 0$; i.e., if the average thickness left in the wake is less than h_0, as seen for the

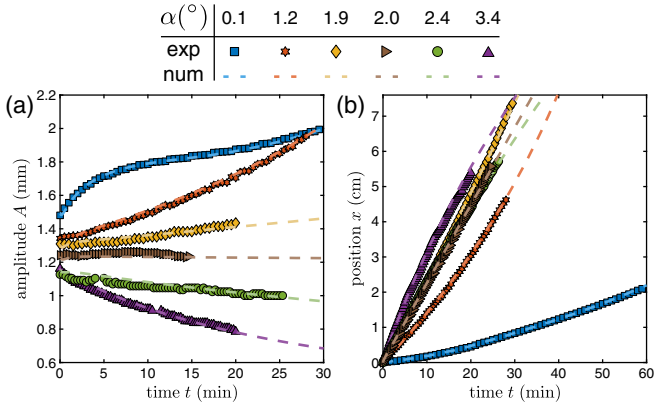

FIG. 3. Shown is the (a) amplitude $A(t)$ and (b) position $x(t)$ of drops sliding under a film of thickness $h_0 \approx 89$ μm at different inclination angles α (see legend). Markers indicate experiments and dashed lines indicate numerical simulations.

greater values of the inclination. The structure of the wake is thus key for rationalizing the transition between the two flow regimes. This numerical observation is confirmed in experiments: as evident from Fig. 4(b), the wake is thinner than h_0 for $\alpha < \alpha_c$ and thicker for $\alpha > \alpha_c$ (see details in the Supplemental Material, Sec. I [23]).

We model the variation in thickness across the wake using an approach analogous to that used in Landau-Levich and Bretherton problems. We treat our problem in the polar coordinate system centered on the drop apex [see Fig. 4(c)]. Focusing on the matching region between the drop and the film, we expect the radial curvature to vary rapidly and dominate the pressure gradient [22]. Consequently, we neglect the advection and gravity terms in the meniscus such that Eq. (1) reduces to a radial Landau-Levich equation (see Supplemental Material, Sec. III [23]). Therefore, we treat the wake as a collection of two-dimensional radial Landau-Levich films, where the projected speed $U\cos(\theta)$ is the effective deposition speed. In this framework, we obtain [25]

$$h_w(\theta) \approx 1.34\kappa_d^{-1}\cos(\theta)^{2/3}\mathrm{Ca}^{2/3}. \quad (2)$$

Here κ_d is the curvature at the edge of the drop, which is assumed to remain close to that of a static pendant drop $\kappa_d \approx 0.28A/\ell_c^2$ (see Supplemental Material, Sec. III [23]), and $\mathrm{Ca} = \eta U/\gamma$ is the capillary number of the problem. Note that the drop speed $U(t)$ and amplitude $A(t)$ are *a priori* unknown and depend on the drop initial profile, film thickness, and inclination of the substrate. Varying the dimensionless parameters of the problem (A_0/ℓ_c, h_0/ℓ_c, and $\tilde{\alpha}$), we generate a large dataset of simulations to assess the validity of our model.

In Fig. 5(a), we plot the wake profile in the transverse direction $h_w(y)$ for a given drop and film at different inclination angles [the wake is quasi-invariant in the x direction, see Fig. 4(a)]. We first focus on the angular dependence by rescaling the data by $h_w(y=0)$. As shown in Fig. 5(b), the profiles collapse in the central region of the wake defined as $-R < y < R$ with R the drop radius. The resulting master curve matches our theoretical prediction $h_w(\theta)/h_w(0) = \cos(\theta)^{2/3}$ with no fitting parameter [see Eq. (2)]. We then compare our prediction for $h_w(0)$ to data from all our simulations in Fig. 5(c). Note that each simulation provides multiple data points, as A and U are both functions of time and thus vary over the course of a simulation. The resulting collapse and overall favorable agreement with Eq. (2) confirms the validity of our approach. Note that the agreement becomes less favorable when $\tilde{\alpha}$ and h_0/ℓ_c increase, a result consistent with the approximations made in our model (negligible advection in the meniscus and static pendant drop shape, see Supplemental Material, Sec. III [23]).

Using Eq. (2), we evaluate the amount of liquid deposited in the wake $\int_{-R}^{R} h_w(y)dy = Rh_w(0)\int_{-\pi/2}^{\pi/2}\cos(\theta)^{5/3}d\theta$ and obtain the drop growth rate

$$\partial_x V \approx R(2h_0 - 7.91\ell_c^2\mathrm{Ca}^{2/3}/A). \quad (3)$$

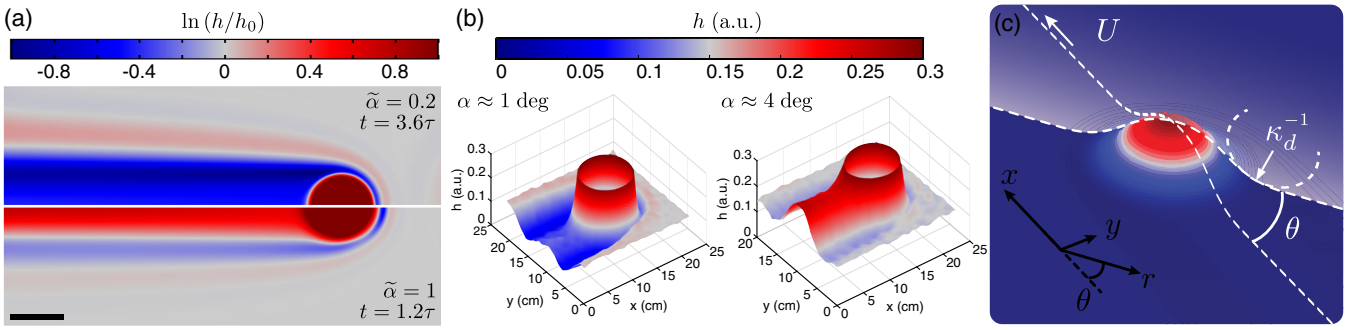

FIG. 4. (a) Thickness map for two simulations with identical initial drops ($A_0/\ell_c = 1.05$, $h_0/\ell_c = 0.04$) but different inclination angles $\tilde{\alpha}$ (position $x = 37.4\ell_c$). Scale bar $5\ell_c$. (b) Thickness profiles inferred from experiments conducted with dyed oil at low and high inclination angles ($A_0/\ell_c \approx 0.8$, $h_0 \approx 85$ μm). (c) Three-dimensional schematics of the drop introducing the polar coordinates $\{r, \theta\}$ and curvature κ_d.

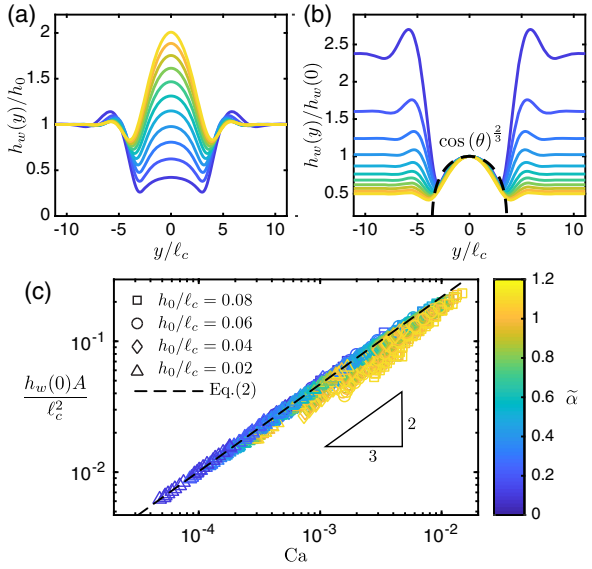

FIG. 5. (a) Wake profile $h_w(y)/h_0$ taken $\approx 6\ell_c$ behind a drop [23] for different inclination angles $\tilde{\alpha}$ [color coded, see (c)], $A_0/\ell_c = 1.4$ and $h_0/\ell_c = 0.04$. (b) Same data rescaled by the central thickness $h_w(0)$. The black dashed line derives from Eq. (2): $h_w(y)/h(0) = \cos(\theta)^{2/3} = \cos[\arcsin(y/R)]^{2/3}$. (c) Dimensionless thickness in the center of the wake $h_w(0)A/\ell_c^2$ as a function of the capillary number Ca for our 176 simulations. The color codes $\tilde{\alpha}$, the symbols code h_0/ℓ_c, and the black dashed line corresponds to Eq. (2): $y = 1.34/0.28x^{2/3}$.

Next, we derive an expression for Ca in order to close the problem.

To obtain the drop speed, we perform a force balance on the drop [26]. The force driving the motion of the drop derives from the change in gravitational energy $E_p = \rho g V z_c$, with z_c as the altitude of the drop center of mass. Defining $F_g = -\partial_x E_p$, we find $F_g \approx \rho g V \alpha + 2\rho g z_c R h_0 - 7.91\gamma R z_c \mathrm{Ca}^{2/3}/A$. Whereas the first term in the expression of F_g is conventional, the other two terms originate from the change of volume of the drop $\partial_x V$ in Eq. (3). The motion of the drop is resisted by viscous stresses in the film. The flow being significant only around the drop and the meniscus being the thinnest part of that region, we anticipate the meniscus to be the main source of dissipation. The corresponding viscous force per unit length is $f_v(\theta) = 4.94\gamma(\mathrm{Ca}\cos\theta)^{2/3}$ [25]. Integrating along the drop contour, the total friction force is $\mathbf{F_v} = \int_{-\pi/2}^{\pi/2} f_v(\theta)(\cos\theta \mathbf{e_x} + \sin\theta \mathbf{e_y}) R d\theta \approx 8.31\gamma R \mathrm{Ca}^{2/3}\mathbf{e_x}$. Assuming that the drop shape remains close to that of a static pendant drop, we have $z_c \approx 0.29A$, $R \approx 3.58\ell_c$, and $V \approx 0.89AR^2$ (see Supplemental Material, Sec. III [23] for the derivation of all the prefactors). Balancing F_g and $F_v = \mathbf{F_v}\cdot\mathbf{e_x}$, we obtain

$$\mathrm{Ca}^{2/3} = 0.0553\frac{Ah_0}{\ell_c^2}(1 + 5.34\tilde{\alpha}). \tag{4}$$

In Fig. 6(a), we compare the drop speed obtained in simulations with Eq. (4) and find favorable agreement without any fitting parameter. Likewise, we show in the inset of Fig. 6(a) that Eq. (4) also captures our experiments. Note that the agreement becomes less favorable when $\tilde{\alpha}$ and h_0/ℓ_c increase, as expected from the deterioration of our model's assumptions (static pendant drop shape and negligible advection in the meniscus, see Supplemental Material, Sec. III [23]).

We now leverage our results and combine Eqs. (3) and (4) to derive the drop growth rate $\partial_x V$ and subsequently integrate this expression over time to obtain the drop dimensionless amplitude

$$\frac{\bar{A}(\bar{t})}{\bar{A}_0} = \left(1 - \frac{1}{2}f(\tilde{\alpha})\bar{A}_0^{1/2}\bar{t}\right)^{-2} \tag{5}$$

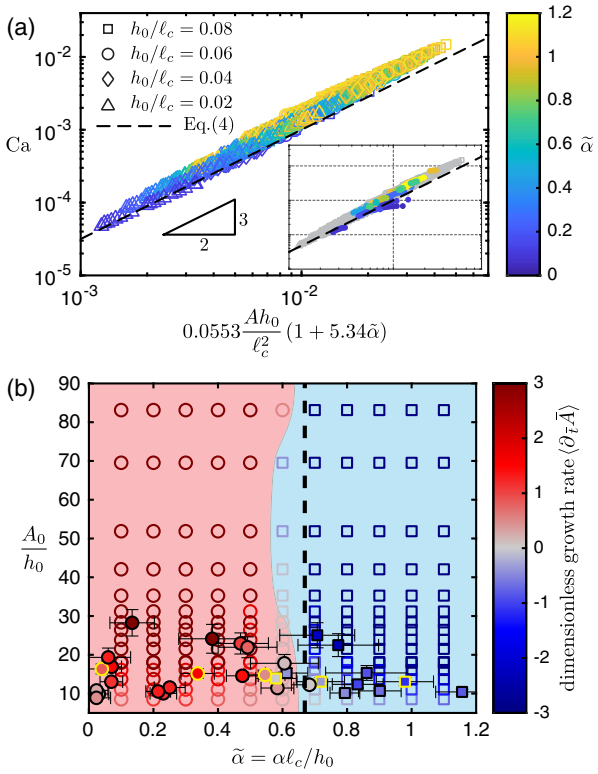

FIG. 6. (a) Drop dimensionless speed Ca compared to our theory [Eq. (4)]. Our 176 simulations are shown, the color codes $\tilde{\alpha}$, the symbols code h_0/ℓ_c, and the black dashed line is our prediction $y = x^{3/2}$. Inset: same plot including experimental data ($0.03 < h_0/\ell_c < 0.1$). The numerics are drawn in light gray for clarity. (b) State diagram for the drop dynamics. Symbols are colored according to the average dimensionless growth rate, $\langle\partial_{\bar{t}}\bar{A}\rangle$, evaluated over the course of the experiment or the simulation depending on the case. Circles represent growth ($\langle\partial_{\bar{t}}\bar{A}\rangle > 0$), while squares represent decay ($\langle\partial_{\bar{t}}\bar{A}\rangle < 0$). Experimental results are shown as filled symbols, while numerical results are open symbols. The experiments of Fig. 3 are circled in yellow. The background color is a guide to the eye and the dashed black line is our theory $\tilde{\alpha}_c \approx 0.67$.

with $f(\tilde{\alpha}) = (0.0065 - 0.0097\tilde{\alpha})(1 + 5.34\tilde{\alpha})^{3/2}$ (see Supplemental Material, Sec. III [23]). In Fig. S5(a), we show that Eq. (5) compares favorably with experiments without fitting parameters. The value of the critical inclination is obtained solving for the root of f, yielding $\tilde{\alpha}_c \approx 0.67$. In Fig. 6(b), we show the combined experimental and numerical state diagram for the drop dynamics, where the two flow regimes are apparent. As predicted by our model, the transition occurs at a roughly constant critical angle $\tilde{\alpha}_c \approx 0.6$ in good agreement with our estimate.

In summary, using experiments and numerical simulations, we have revealed a transition from growth to decay for pendant drops sliding under slightly inclined prewet substrates. This transition, which occurs at a surprisingly low angle, is governed by the amount of fluid left in the wake of the drop. As the inclination angle increases, the drop becomes too fast to grow and its volume is slowly depleted. We have rationalized this complex nonlinear problem with an analytically tractable Landau-Levich model that accurately predicts the drop dynamics in the two regimes, in spite of the approximations introduced in its derivation. Note that on longer timescales the Rayleigh-Taylor instability will eventually influence the dynamics of drops that do not drip. Although this situation is beyond the scope of the present Letter, preliminary results indicate that the wake forms lenses that are later absorbed by the drop (see Supplemental Material, Sec. II [23] and Video S3). Yet, no dripping is observed, which suggests that the critical angle we have introduced remains accurate. As such, our results could find application in dripping prevention for drops directly deposited on substrates, e.g., in coating and printing technologies [27]. Additionally, our results could be extended to control and transport pendant drops via carefully crafted substrate topography. Finally, our analysis could be generalized to model the dynamics of sliding liquid plugs in prewetted channels [28] and sliding liquid bridges between prewetted substrates [29,30].

We thank P. Bourrianne for measuring the silicone oil viscosity. E. J.-P. was partially supported by NSF through the Princeton University's Materials Research Science and Engineering Center DMR-1420541 and the Princeton Yang Family and David T. Wilkinson Innovation Funds. P. G. L. acknowledges the Swiss National Science Foundation under Grant No. 200021-178971.

[1] S. G. Yiantsios and B. G. Higgins, Rayleigh-Taylor instability in thin viscous films, Phys. Fluids A **1**, 1484 (1989).
[2] M. Fermigier, L. Limat, J. E. Wesfreid, P. Boudinet, and C. Quilliet, Two-dimensional patterns in Rayleigh-Taylor instability of a thin layer, J. Fluid Mech. **236**, 349 (1992).
[3] R. T. Weitz, L. Harnau, S. Rauschenbach, M. Burghard, and K. Kern, Polymer nanofibers via nozzle-free centrifugal spinning, Nano Lett. **8**, 1187 (2008).
[4] J. Marthelot, E. F. Strong, P. M. Reis, and P.-T. Brun, Designing soft materials with interfacial instabilities in liquid films, Nat. Commun. **9**, 4477 (2018).
[5] E. Jambon-Puillet, M. Royer Piéchaud, and P.-T. Brun, Elastic amplification of the Rayleigh-Taylor instability in solidifying melts, Proc. Natl. Acad. Sci. U.S.A. **118**, e2020701118 (2021).
[6] N. Ribe, A. Davaille, and U. Christensen, Fluid dynamics of mantle plumes, in *Mantle Plumes: A Multidisciplinary Approach*, edited by J. R. R. Ritter and U. R. Christensen (Springer, Berlin, Heidelberg, 2007), pp. 1–48.
[7] C. Camporeale and L. Ridolfi, Hydrodynamic-Driven Stability Analysis of Morphological Patterns on Stalactites and Implications for Cave Paleoflow Reconstructions, Phys. Rev. Lett. **108**, 238501 (2012).
[8] U. Dutta, A. Baruah, and N. Mandal, Role of source-layer tilts in the axi-asymmetric growth of diapirs triggered by a Rayleigh–Taylor instability, Geophys. J. Int. **206**, 1814 (2016).
[9] S. J. Weinstein and K. J. Ruschak, Coating flows, Annu. Rev. Fluid Mech. **36**, 29 (2004).
[10] R. Kaita *et al.*, Experiments with liquid metal walls: Status of the lithium tokamak experiment, Fusion Eng. Des. **85**, 874 (2010).
[11] G. G. van Eden, V. Kvon, M. C. M. van de Sanden, and T. W. Morgan, Oscillatory vapour shielding of liquid metal walls in nuclear fusion devices, Nat. Commun. **8**, 192 (2017).
[12] L. Limat, P. Jenffer, B. Dagens, E. Touron, M. Fermigier, and J. Wesfreid, Gravitational instabilities of thin liquid layers: Dynamics of pattern selection, Physica (Amsterdam) **D61**, 166 (1992).
[13] H. N. Yoshikawa, C. Mathis, S. Satoh, and Y. Tasaka, Inwardly Rotating Spirals in a Nonoscillatory Medium, Phys. Rev. Lett. **122**, 014502 (2019).
[14] G. Lerisson, P. G. Ledda, G. Balestra, and F. Gallaire, Instability of a thin viscous film flowing under an inclined substrate: Steady patterns, J. Fluid Mech. **898**, A6 (2020).
[15] J. M. Burgess, A. Juel, W. D. McCormick, J. B. Swift, and H. L. Swinney, Suppression of Dripping from a Ceiling, Phys. Rev. Lett. **86**, 1203 (2001).
[16] V. Lapuerta, F. J. Mancebo, and J. M. Vega, Control of Rayleigh–Taylor instability by vertical vibration in large aspect ratio containers, Phys. Rev. E **64**, 016318 (2001).
[17] A. Alexeev and A. Oron, Suppression of the Rayleigh–Taylor instability of thin liquid films by the Marangoni effect, Phys. Fluids **19**, 082101 (2007).
[18] R. Cimpeanu, D. T. Papageorgiou, and P. G. Petropoulos, On the control and suppression of the Rayleigh–Taylor instability using electric fields, Phys. Fluids **26**, 022105 (2014).
[19] P. H. Trinh, H. Kim, N. Hammoud, P. D. Howell, S. J. Chapman, and H. A. Stone, Curvature suppresses the Rayleigh–Taylor instability, Phys. Fluids **26**, 051704 (2014).
[20] P.-T. Brun, A. Damiano, P. Rieu, G. Balestra, and F. Gallaire, Rayleigh–Taylor instability under an inclined plane, Phys. Fluids **27**, 084107 (2015).

[21] G. Balestra, N. Kofman, P.-T. Brun, B. Scheid, and F. Gallaire, Three-dimensional Rayleigh–Taylor instability under a unidirectional curved substrate, J. Fluid Mech. **837**, 19 (2018).
[22] J. R. Lister, J. M. Rallison, and S. J. Rees, The nonlinear dynamics of pendent drops on a thin film coating the underside of a ceiling, J. Fluid Mech. **647**, 239 (2010).
[23] See Supplemental Material at http://link.aps.org/supplemental/10.1103/PhysRevLett.127.044503 for experimental and numerical methods, additional experimental and numerical results, and more details about the model and its limitations.
[24] S. D. R. Wilson, The drag-out problem in film coating theory, J. Eng. Math. **16**, 209 (1982).
[25] I. Cantat, Liquid meniscus friction on a wet plate: Bubbles, lamellae, and foams, Phys. Fluids **25**, 031303 (2013).
[26] P. Aussillous and D. Quéré, Bubbles creeping in a viscous liquid along a slightly inclined plane, Europhys. Lett. **59**, 370 (2002).
[27] S. Kumar, Liquid transfer in printing processes: Liquid bridges with moving contact lines, Annu. Rev. Fluid Mech. **47**, 67 (2015).
[28] J. Bico and D. Quéré, Self-propelling slugs, J. Fluid Mech. **467**, 101 (2002).
[29] E. Reyssat, Drops and bubbles in wedges, J. Fluid Mech. **748**, 641 (2014).
[30] G. M. N. Balestra, Pattern formation in thin liquid films: From coating-flow instabilities to microfluidic droplets, Ph.D. thesis, Lausanne, 2018.